A Rheological Investigation of Entanglement in Side-Chain Liquid-Crystalline Azobenzene Polymethacrylates

ARTICLE *in* MACROMOLECULES · JUNE 2013

Impact Factor: 5.8 · DOI: 10.1021/ma400260n

4 AUTHORS, INCLUDING:

Laura Andreozzi
Università di Pisa
94 PUBLICATIONS **835** CITATIONS
SEE PROFILE

Michele Giordano
Italian National Research Council
429 PUBLICATIONS **4,781** CITATIONS
SEE PROFILE

Macromolecules

Article

pubs.acs.org/Macromolecules

A Rheological Investigation of Entanglement in Side-Chain Liquid-Crystalline Azobenzene Polymethacrylates

L. Andreozzi,*[,†,§] G. Galli,[‡] M. Giordano,[†,§] and F. Zulli[†,§]

[†]Department of Physics "E. Fermi", University of Pisa, Pisa, Italy

[§]IPCF-CNR, Pisa, Italy

[‡]Department of Chemistry and Industrial Chemistry and INSTM, University of Pisa, Pisa, Italy

Supporting Information

ABSTRACT: The shear rheological behavior was investigated in a series of high molar mass liquid-crystalline polymers (PMA4 homopolymer and copolymer samples) carrying an azobenzene mesogenic group in the side chains (MA4). The focus was on studying the entanglement effects and testing selected reptation models to ascertain their ability to reproduce the complex shear modulus of the copolymers. We found that ordinary dynamic models worked for the nematic PMA4 copolymers with methyl methacrylate (MMA), nicely reproducing the rheological response of the materials. We were able to obtain microscopic information on the materials, such as Rouse time and entanglement molar mass, in a consistent way, as well as to get insight on the macroscopic effects of tube dilatation induced by the nematic order on the master curves of the entangled polymers. Model improvements, accounting for the different nature of the counits, were also proposed in this work that singled out the friction coefficients of the counits MMA and MA4. The monomeric friction coefficient ζ_0^{MA4} was found to be constant throughout the series, $(5 \pm 2) \times 10^{-9}$ kg s^{-1}. Likewise, ζ_0^{MMA} had the same value throughout the series, very similar to literature data for PMMA homopolymers, $(2.0 \pm 0.6) \times 10^{-8}$ kg s^{-1}. Finally, in the framework of the packing-length model, constant packing lengths of 3.5 and 13 Å throughout the series were found for MMA and MA4 counits, respectively. Also, it resulted that the viscoelastic behavior of any PMA4 random copolymer could be predicted, provided that the response of the extreme homopolymers of the series has been characterized.

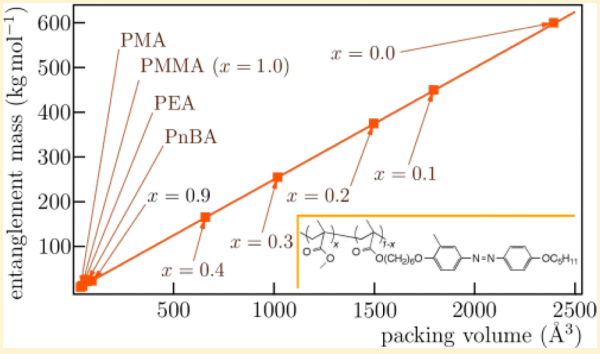

1. INTRODUCTION

Azobenzene-containing polymers have attracted numerous studies of both fundamental significance and practical potential owing to photoresponsiveness of the azobenzene chromophore.[1] Very recent advances span from ferroelectric networks with a photoswitchable second-order nonlinear optical response,[2] to laser-induced holographic light scattering polymers,[3] to hybrid supramolecular materials for processing carbon nanotubes.[4] Specifically, liquid-crystalline azobenzene polymers combine in one macromolecular structure the peculiar characteristics of the molecular mesogenic group with those typical of a polymer architecture. The former include dielectric anisotropy, photochromism and photoalignment via photoselection, while the latter include processing versatility and diversity of mechanical and rheological behaviors.[1] Side-chain liquid-crystalline azobenzene polymers are in fact regarded as suitable candidates as fully optical (nano)writing media.[5] Homogeneity at nano- to microscopic length scale, working temperatures and bit stability have long been recognized as key parameters for effective and long-term storage of optical data.[5,6] In this respect, detailed knowledge of polymer dynamics and its implications at microscopic level on friction and relaxation can help to address implementation of polymer optical media in practical devise application. In particular, topologic properties of the polymer affect both the global dynamic response over larger time-length scales and dynamics of local molecular groups. It appears of interest to understand how the liquid-crystalline order influences the polymer dynamics particularly in presence of high masses, that ensure mechanical and bit stability.[6]

The reptation and tube concepts, first developed by Edwards[7] and de Gennes,[8] are key features that opened the pathway to model with a certain accuracy the dynamics of high polymers. According to these concepts, a topological restriction to molecular motion (entanglement) arises in polymer melts by the presence of other chains, and is characterized by an effective internal scale, the entanglement mass M_e.[9] The entanglements confine the polymer chain motion to a tube. Since polymer chains would have be broken to allow the restricted chain to pass through them, chain diffusion induces the chain to flow outside the tube in a snake-like way.[9]

Received: February 4, 2013
Revised: March 28, 2013
Published: June 10, 2013

Over the years, several models have been developed in the literature to describe the reptation dynamics. Some of them, which resulted oversimplified, limited the effectiveness of the model by considering other relaxation mechanisms besides curvilinear diffusion of a chain in the tube. On the other hand, accounting also for tube length fluctuations, constraint release relaxation, and Rouse-type relaxation of the tube got more insight in the dynamics of entangled linear homopolymers.[10−16] Moreover, mixing rules of these relaxation mechanisms were refined,[12,17,18] in order to obtain quantitative predictions of linear viscoelasticity for melts of polydisperse polymers from the knowledge of the molar mass distribution, while a flurry of studies attempted to answer the question of the best overall model for the dynamics of well entangled linear polymers in melts.[19−21]

Following the success in describing the dynamics of linear polymers melts, dynamic models for nonlinear macromolecular architecture were also developed to describe branched,[22] star,[23] and comb-like[24] polymers. Nonetheless, the validity limits of these models are being still checked out by tests and possible model improvements. For example, severe conditions could be imposed to nonlinear macromolecules by the broadness of molar mass distributions that could lead to nonlinear mixing rules,[25] or even, in the description of dynamics of copolymers, a critical role could be played by the different nature of the counits. Indeed, it is well-known that copolymers can show heterogeneous dynamics leading to nonscalable temperature-dependent relaxation time distributions, in contrast with the previously cited models of polymer dynamics. Exceptions are rare, especially in case of block copolymers because a copolymer relaxes like a chain having uniform friction only when the friction coefficients of the distinct blocks are similar.[26] On the other hand, dealing with random copolymers at not too short time or length scales, homogeneity could be obtained at an extent sufficient to obtain responses that can be mimicked by the ordinary polymer dynamics theories.

In this paper, we report a rheological study carried out on a series of side-chain liquid-crystalline polymers (PMA4). The series includes homopolymers of an azobenzene methacrylate (MA4), with the azobenzene moiety in the side chain, and their random copolymers with different amounts of methyl methacrylate (MMA) counits.

Relatively few studies have appeared in literature dealing with the viscoelastic behavior of side-chain liquid-crystalline polymers, so the aim of this work was both to get more insight in the rheology of these systems, focusing on the entanglement effects, and to test selected reptation models to investigate their ability in reproducing the complex shear modulus of the copolymer series. Besides the copolymer nature of this system, their liquid-crystalline nature offers a further test of polymer dynamic models, because these copolymers did not show any entanglement plateau despite their molar masses, much higher than the ones of well-entangled ordinary polymers.

In spite of all these peculiar features of the polymer series, we found that ordinary dynamic models worked for the PMA4 copolymers, and we evidenced that the nematic order, proper of most of the investigated polymers of the series, dilates the reptation tube and shifts entanglement mass toward higher values with respect to linear polymer. The analysis of reptation dynamics on PMA4 was completed using MML model to calculate viscosity. Improvements, accounting for the different nature of the counits, are discussed, which also allowed the determination of the monomeric friction coefficients of the counits. Moreover, the insertion of PMA4 in the framework of the packing-length model suggested the possibility to predict the viscoelastic behavior of whatever PMA4 random copolymer, provided that the responses of the parent homopolymers of the series have been characterized.

2. THEORETICAL BACKGROUND

In this paper, the complex shear modulus of PMA4 melts is calculated, combining Rouse model and Doi−Edwards theory[10] for viscoelasticity and entanglement dynamics in polymers. More models and mechanisms for relaxation are also taken in consideration and discussed, such as contour length fluctuation and constraint release relaxation.[10] The original form of all these literature models is here modified by means of a weighted monomeric friction coefficient to account for the random nature of PMA4 copolymers. In the following, only the results of the models relevant to the present work are reported. More details can be found in literature.[10,12−17,19,20,27−29]

According to the Rouse theory for unentangled chains (UR), at temperature T the shear relaxation modulus of a monodisperse melt with molar mass M can be written as a function of the time t as[10]

$$G(t) = \frac{\rho N_A k_B T}{M} \sum_{p>0} \exp\left(-\frac{2p^2 t}{\tau_R}\right) = \frac{\rho N_A k_B T}{M} m_{UR}(t) \quad (1)$$

In eq 1, $m_{UR}(t)$ is the relaxation function, ρ is the density of the melt, N_A is the Avogadro number, k_B the Boltzmann constant, and τ_R is the Rouse relaxation time, which in turn depends on the monomeric friction coefficient ζ_0, the length b and the number N of chain segments according to[10]

$$\tau_R = \frac{\zeta_0 N^2 b^2}{3\pi^2 k_B T} = K_R N^2 \quad (2)$$

In eq 2, K_R is a parameter independent of the molar mass M (i.e., N).

When the macromolecules in the melt are not constrained by entanglements ($M < M_e$, the entanglement mass), the relaxation results from monomer friction only and is described by the Rouse mechanism. Also in entangled polymers, the relaxation processes at a time much shorter than a characteristic time for reptation, the reptation time, are dominated by the Rouse mechanism.[10] However, a significant difference is found for the Rouse relaxation of entangled polymer melts with respect to unentangled ones: at times about the entanglement time[29,30] $\tau_e = \tau_R M_e^2/M^2$ or greater, those modes given by subchains with molar mass lower than M_e are relaxed, while the Rouse relaxation of longer modes/subchains is hampered by the presence of the reptation tube,[7,8] so that only longitudinal Rouse modes along the tube contribute to the relaxation. This leads to[20]

$$G(t) = \frac{\rho N_A k_B T}{M} \sum_{p>M/M_e} \exp\left(-\frac{2p^2 t}{\tau_R}\right) + \kappa \frac{\rho N_A k_B T}{M} \sum_{p=1}^{M/M_e} \exp\left(-\frac{p^2 t}{\tau_R}\right) = \frac{\rho N_A k_B T}{M} m_{ER}(t) \quad (3)$$

where $m_{ER}(t)$ is the relaxation function of the Rouse modes in entangled chains (ER).

dx.doi.org/10.1021/ma400260n | Macromolecules 2013, 46, 5003−5017

Equation 3 combines the Rouse mechanism of relaxation of "unentangled" subchains (fast modes with $p > M/M_e$ inside the tube) and the relaxation of the slower longitudinal modes. For the latter, in some studies[19,27,28] the empirical factor $\kappa = 1/3$ was used to account for that only one mode over three takes part in the relaxation. Other studies[20] provided a different value of $\kappa = 1/5$. This means that 1/5 of the stress stored in the tube is relaxed after a time τ_R by longitudinal modes. At τ_R, the residual fraction of the stress is therefore supplied by unrelaxed mechanisms, such as reptative relaxations. In this paper, we will refer to the model of eq 3 as ER3 or ER5 depending on the employed value of κ, 1/3 or 1/5 respectively.

Several models have been proposed in the literature to describe the reptative dynamics of entangled linear chains. According to the first quantitative description by Doi and Edwards,[10] the shear stress modulus in entangled chains (DE) can be expressed as:

$$G(t) = \frac{\rho N_A k_B T}{M_e}\frac{8}{\pi^2}\sum_{p:\text{odd}}\frac{1}{p^2}\exp\left(-\frac{p^2 t}{\tau_d}\right) = G_0^N m_{\text{DE}}(t) \tag{4}$$

In eq 4, G_0^N is the plateau modulus, $m_{\text{DE}}(t)$ the relaxation function. τ_d is the disengagement time, or reptation time, and is the time for the chain to renew its configuration and to escape from the tube. τ_d is also the longest relaxation time of the polymer melt. It is given by:[29,30]

$$\tau_d = \frac{\zeta_0 N^3 b^4}{\pi^2 k_B T a^2} = 3\frac{Nb^2}{a^2}\tau_R = 3\frac{M}{M_e}\tau_R \tag{5}$$

where a is the tube diameter.

It is seen from eq 5 that DE model yields to $\tau_d \propto M^3$, which is not equal, but quite close, to the experimental result of $\tau_d \propto M^{3.4}$. To recover the $\tau_d \propto M^{3.4}$ experimental dependence of the entangled polymer melts, the DE relaxation function can be modified to include fluctuations of the tube length around its equilibrium value. This leads to an expression for $G(t)$ (DECLF) as[10,19]

$$G(t) = \frac{\rho N_A k_B T}{M_e}\int_0^1 \exp\left(-\frac{t}{\tau(\xi)}\right)\mathrm{d}\xi = G_0^N m_{\text{DECLF}}(t) \tag{6}$$

with

$$\tau(\xi) = \frac{\xi^4}{4\xi_{cr}^2}\tau_d, \quad 0 < \xi < \xi_{cr} \tag{7a}$$

$$\tau(\xi) = \left(\xi - \frac{\xi_{cr}}{2}\right)^2\tau_d, \quad \xi_{cr} < \xi < 1 \tag{7b}$$

$$\xi_{cr} = 2\nu\sqrt{\frac{M_e}{M}} \tag{7c}$$

that is just constructed to merge the fluctuations at short time scale with the reptation at long times, discriminated by ξ_{cr}.[10] Equation 7c expresses ξ_{cr} in terms of the molar mass, the entanglement mass and the parameter ν, that depends on the material.[19]

The contour length fluctuations are also semiempirically accounted for by another development of the DE theory, the time-dependent diffusion model (TDD),[12] which provides

$$G(t) = \frac{\rho N_A k_B T}{M_e}\frac{8}{\pi^2}\sum_{p:\text{odd}}\frac{1}{p^2}\exp\left(-p^2\left(\frac{t}{\tau_d} - \frac{M_d}{M}g\left(\frac{Mt}{M_d\tau_d}\right)\right)\right) = G_0^N m_{\text{TDD}}(t) \tag{8}$$

In this formula, $m_{\text{TDD}}(t)$ is the TDD relaxation function, M_d is an empirical parameter and g is defined according to[12]

$$g(x) = \sum_{k>0}\frac{1 - \mathrm{e}^{-kx^2}}{k^2} \approx -x + x^{0.5}(x + (\pi x)^{0.5} + \pi)^{0.5} \tag{9}$$

As a general remark, the tube model assumes an immobile tube. Indeed this assumption is an oversimplification: the tube constraints are themselves chains that are also reptating, having therefore a finite lifetime. The constraint release (CR) mechanism overcomes this drawback of the tube model, and can be included as a relaxation way for the chains, applying the double reptation scheme[12,13] to the DE, DECLF, and TDD models. The semiempirical approach of double reptation explicitly describes entanglements as binary events.[12,13] The intuitive idea behind it is that an entanglement disappears, and hence a constraint is released, whenever a chain end passes beyond the entanglement. For monodisperse polymer melts, the stress relaxation function within the double reptation theory is proportional to the square of $m(t)$ according to[11,12]

$$G_{\text{double}}(t) = G_0^N m_{\text{single}}{}^2(t) \tag{10}$$

where $m_{\text{single}}(t)$ is the shear modulus relaxation function of single reptation models without the CR mechanism (e.g., eqs 4, 6, and 8).

Then, the total shear relaxation modulus $G(t)$ of the monodisperse polymer melt can be obtained as a sum of the different contributions chosen to model the relaxation:

$$G(t, M) = G_0^N m_{\text{single}}^{\beta}(t, M) + \frac{\rho N_A k_B T}{M} m_{\text{Rouse}}(t, M) \tag{11}$$

The exponent β accounts for the CR mechanisms, $m_{\text{single}}(t, M)$ is shear modulus relaxation function of single reptation models of the monodisperse polymer of mass M, as for eq 10. The $m_{\text{Rouse}}(t, M)$ provides the Rouse relaxation of the polymer chains, and corresponds to $m_{\text{ER}}(t)$ or $m_{\text{UR}}(t)$ for entangled or unentangled chains, respectively.

On the other hand, polydisperse polymers can be profitably handled taking into proper account the contributions to $G(t, M)$ of all monodisperse components of mass M of the molar mass distribution $w(M)$ of the melt

$$w(M) = \frac{\mathrm{d}[W(M)]}{\mathrm{d}[\log M]} \tag{12}$$

where $W(M)$ is the weight fraction of chains with molar mass lower than M. Accordingly, the overall relaxation modulus can be written in the general mixing rule form[17,19]

$$G(t) = G_0^N\left(\int_{\log M_i}^{\log M_f} m_{\text{single}}(t, M)w(M)\,\mathrm{d}[\log M]\right)^{\beta} + \frac{\rho N_A k_B T}{M}\int_{\log M_i}^{\log M_f} m_{\text{Rouse}}(t, M)w(M)\,\mathrm{d}[\log M] \tag{13}$$

dx.doi.org/10.1021/ma400260n | Macromolecules 2013, 46, 5003−5017

with $m_{single}(t, M)$ and $m_{Rouse}(t, M)$ relaxation functions of the monodisperse polymer of mass M. The values of the extremes of the molar mass range (M_i and M_f) and the value of the exponent $\beta > 0$ are specific to the model describing the monodisperse shear modulus and relaxation function.

To be more specific, it is possible to summarize as follows.

1 For unentangled chains, the sole contribution to eq 13 comes from the Rouse term, with $m_{Rouse} = m_{UR}$, $M_i = 0$, and $M_f = M_e$.
2 For entangled chains, fast and longitudinal Rouse modes of ER contribute to eq 13 with $m_{Rouse} = m_{ER}$, $M_i = M_e$, and $M_f = \infty$.
3 In reptation, simple reptation mechanisms are accounted for by the integral of $m_{single}(t, M)$, with $\beta = 1$, $M_i = M_e$, and $M_f = \infty$. When constraint release mechanisms are described by double reptation theory (eq 10), $M_i = M_e$, $M_f = \infty$, and $\beta = 2$ should be chosen.[12] In particular, $\beta = 2.25$ has been found to be a better value, which also accounts for high order entanglements or could be linked to the tube dilation model.[15]

It is worth noting that in the case $\beta = 1$ (i.e., absence of CR), one could obtain $G^*(\omega)$ from eq 13 analytically.

A further model was proposed in the literature, which combines self-consistent theories for contour length fluctuations and CR mechanisms: the Milner−McLeish−Likhtman (MML) model.[20,28] This model starts from the DE model and unites theoretical and stochastic simulation approaches, adopting a renormalization of the disengagement time to include contour length fluctuation. CR mechanism is added following the scheme proposed by Rubinstein and Colby,[16] that introduces a dimensionless parameter c_v reflecting the "strength" of the constraint release mechanism.

The MML model reduces at minimum the number of free parameters necessary to calculate the linear viscoelastic behavior of entangled polymers, namely M_e, c_v, and K_R, and it resulted to be very effective in simulating the dynamics of nearly monodisperse samples. Some drawbacks could arise in its application to the polymers studied in the present work: indeed MML model, retrieved from and tested on ordinary flexible polymers, could fail for PMA4 polymers, and its efficacy in calculating G^* could be limited because of the PMA4 polydispersity or their liquid-crystalline nature.

In this paper, we compare the outcomes of some of the models presented here, then reporting for the reptation dynamics calculations according to the DECLF model, which was preferred to the DE and TDD models because it does not contain empirical parameters. In addition, the TDD model is known to be unable to correctly predict relaxation of short chains.[19] The analysis of reptation dynamics on PMA4 will be completed using MML model to calculate viscosity. A complete test on PMA4 entanglement dynamics with MML model will be postponed to a later work.

3. EXPERIMENTAL SECTION

3.1. Synthesis. The polymer system under investigation, referred to as PMA4, consisted of two homopolymer samples (S1 and S5) of a nematogenic azobenzene methacrylate (MA4)[31,32] and five random copolymer samples (C1−C4 and C9) of MA4 and methyl methacrylate (MMA) with different molar compositions (Figure 1). The composition of the copolymers was determined from the integrated areas of the ^{1}H NMR well resolved signals of the $COOCH_3$ protons of the MMA counits (at 3.6 ppm) and the OCH_2 protons of the MA4 counits (at 3.9−4.1 ppm). A PMMA homopolymer sample was also studied for comparison. The MA4 repeat unit has a molar mass of 468 g mol^{-1} and a side-chain length of about 30 Å.[33] The MMA repeat unit has a molar mass of 100 g mol^{-1} and a side-chain length of about 2.5 Å.[33] Incorporation of the mesogenic azobenzene side-chain group via a hexamethylene spacer[34] into the polymethacrylate main-chain backbone of PMA4 was necessary to ensure formation of a nematic mesophase, without intervention of a smectic mesophase or a semicrystalline phase above the glassy state.[34,35]

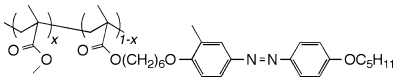

Figure 1. General sketch of the polymer samples investigated with their mole fraction x: PMA4 homopolymers ($x = 0$), PMMA homopolymer ($x = 1$), and their random copolymers ($x = 0.1$, 0.2, 0.3, 0.4, 0.9).

3.2. Molar Mass Distribution and Thermal Characterization. Average molar masses and molar-mass distributions were determined either by size-exclusion chromatography (SEC) of chloroform solutions with a Waters 590 chromatograph, equipped with two Shodex KF804 columns and both Waters R401 differential refractive index and PerkinElmer LC75 ultraviolet detectors, or by SEC of chloroform and tetrahydrofuran solutions with a JASCO PU-1580-CO2 chromatograph, equipped with two PLgel 0.005 mm MIXED-C and MIXED-D columns and with both JASCO 830-RI differential refractive index and PerkinElmer LC75 ultraviolet detectors. Standard samples of polystyrene (molar mass in the range of 1−500 kg mol^{-1}) were used for calibration. Average molar masses of PMA4s are given in Table 1. On the basis of our previous findings on measurements of molar masses of MMA-MA4 random and block copolymers by NMR and light scattering methods, we estimate that the absolute values of the molar masses in the distribution of the present polymer samples may differ by 10% from the respective SEC values. It appears that the average molar masses of all PMA4s are greater than the entanglement mass of PMMA homopolymer (about 10 kg mol^{-1}).[36]

Table 1. Physico-Chemical Characterization of PMA4 Polymer Samples

sample	x	M_n (kg mol^{-1})	M_w (kg mol^{-1})	M_w/M_n	$T_g{}^a$ (K)	$T_c{}^a$ (K)	$T_{ni}{}^a$ (K)
S1	0.0	18.6	59.0	3.17	294	320	353
S5	0.0	29.9	72.6	2.43	305	337	357
C1	0.1	53.0	180.0	3.61	306	–	353
C2	0.2	49.0	177.0	3.40	308	–	352
C3	0.3	33.0	117.0	3.54	314	–	348
C4	0.4	23.3	93.2	4.01	320	–	353^b
C9	0.9	21.9	57.3	2.62	356	–	–

^{a}Glass, conformational and nematic-to-isotropic transition temperatures, by DSC. ^{b}The T_{ni} of C4 cannot be measured by DSC, but can be inferred by ESR measurements as a dynamic transition at about 353 K as shown in ref 40.

Differential scanning calorimetry (DSC) characterization was carried out with a PerkinElmer DSC7 apparatus, recording thermograms on heating at 10 K min^{-1} after rapid cooling at 40 K min^{-1} from about 383 K. A glass transition temperature T_g was detected in all samples. A nematic-to-isotropic transition temperature T_{ni} was found for homopolymers S1 and S5 and copolymers C1, C2, and C3 only. A conformational transition was also detected for the two homopolymers due to changes in mobility and topological disorder of the polymer backbone of PMA4 homopolymers.[31,37,38]

From DSC heating scans,[37] the glass transition at T_g was determined according to the enthalpic definition,[39] the nematic-to-isotropic transition at T_{ni} was measured with the onset definition. Transition temperatures are given in Table 1. As the content of MA4 counits decreases in the copolymers, the weakening of the nematic

dx.doi.org/10.1021/ma400260n | Macromolecules 2013, 46, 5003−5017

potential ultimately leads to disappearance of a macroscopic signature of the nematic phase in the C4 and C9 samples. Nonetheless, ESR measurements on C4 signal a dynamic transition at 353 K, which recalls the dynamic transitions found with ESR at T_{ni} for S1, C3, C2, and C1 samples.[40] This suggests that a sort of order is still present at nanolength scale in C4. Such an order was not detected in C9.

3.3. Rheological Characterization. Viscoelastic characterization was performed with oscillatory and creep-recovery experiments, by using a Haake RheoStress 150H torsional rheometer, equipped with a Haake TC501 temperature control system and with parallel-plate sensor system (20 mm diameter). To account for thermal dilatation of the system, the gap between plates was automatically varied with temperature in the range 0.400−0.600 mm. All measurements were gap-independent. The investigated temperatures ranged from about T_g, across the nematic phase, up to well above T_{ni}. The intensities of applied stress were chosen to carry out measurements in regime of linear response. The range of strain corresponding to the linear viscoelastic response was quite broad, even in the nematic phase.

Steady-state viscosity, creep, and creep-recovery experiments were carried out in order to evaluate zero-shear viscosity.[41] In steady-state viscosity experiments (flow curves) the viscosity is measured at any selected shear-rate value until a constant value is obtained. On the other hand, combined use of creep and recovery experiments allows the evaluation of the viscosity of the materials without breaking the linear viscoelastic limit.[41,42] In this work, the occurrence of linear viscoelastic regime was tested by verifying that, at fixed temperatures, the compliance $J(t)$, obtained by a series of creep-recovery experiments for each sample, was independent of the applied stresses.

In oscillatory experiments, isothermal frequency sweeps were usually performed in the range 10^{-3} Hz to 24.4 Hz. However, on approaching the T_g, the lower limit was extended down to 1×10^{-4} Hz. *A posteriori* tests about working within linear viscoelastic conditions were successfully performed, obtaining the same values of the complex modulus $G^*(\omega,T)$ for frequency sweeps where stress/strain measurement conditions were varied suitably. From oscillatory experiments, zero-shear viscosity was obtained according to the relationship: $\eta_0 = \lim_{\omega\to 0} G''/\omega$.[41,43] G'' is the loss modulus, which is defined, together with the shear modulus G', as $G^* = G' + iG''$, where $i^2 = -1$.

Importantly enough, for each characterized sample, the frequency sweeps recorded at different temperatures could be superimposed on single master curves at a reference temperature T_r by horizontal $a_{T_r}(T)$ and vertical $b_{T_r}(T) \cong 1$ shifts according to:[36,44]

$$G^*(\omega/a_{T_r}(T),\ T) = b_{T_r}(T)G^*(\omega,\ T_r) \tag{14}$$

This allowed us to confirm the validity of time-temperature superposition principle (TTS)[45] in PMA4s over the investigated range of frequencies and temperatures. Grounds for occurrence of TTS will be discussed later herein. A specific numerical algorithm[44] was used to shift mathematically the isothermal frequency sweeps, that led to the calculation of master curves of the complex shear modulus $G^*(\omega)$, together with horizontal and vertical shift factors at the reference temperatures T_r.

Theoretical calculations of $G_{th}^*(\omega)$ master curves were elaborated according to the dynamic models described in the theoretical section. Different strategies were adopted to obtain the $G_{th}^*(\omega)$ function in the angular frequency domain starting from the summation of reptation and Rouse contributions in the time domain, as described previously. For Rouse relaxation, the dynamic modulus was obtained analytically, Fourier-transforming eq 1 or eq 3. On the other hand, the complex modulus of reptation models was obtained by Schwarzl approximations,[46] which were preferred over the numerical Fourier transform approach because of their simplicity and the associated computational speed.

To make a quantitative comparison between theoretical and experimental master curves, the reduced χ_r^2 function

$$\chi_r^2 = \frac{1}{N-2}\sum_{k=1}^{N}\left(\frac{\log(G_{exp}'(\omega_k)/G_{th}'(\omega_k))}{\sigma}\right)^2 + \left(\frac{\log(G_{exp}''(\omega_k)/G_{th}''(\omega_k))}{\sigma}\right)^2 \tag{15}$$

was minimized by means of a numerical algorithm implemented on purpose, fitting experimental curves of $G_{exp}^*(\omega)$ according to Nelder−Mead routines[47] over N points. A global maximum relative error of σ = 10% was used in the minimization.

4. RESULTS AND DISCUSSION

4.1. Linear Viscoelastic Characterization. The zero-shear viscosity was determined as a function of the temperature by means of flow curves, creep-recovery, and frequency sweep experiments. The temperature dependence of the viscosity of PMA4 polymers is shown in Figure 2. No discontinuity is detectable, not even in the copolymers across T_{ni}. The continuity of the viscosity across the T_{ni} is consistent with literature results,[48−50] and with dielectric spectroscopy experiments[51] on side-chain liquid-crystalline polymers, confirming how the dynamic consequences of the isotropic-nematic transition are not as severe as for the isotropic-smectic transition.[50]

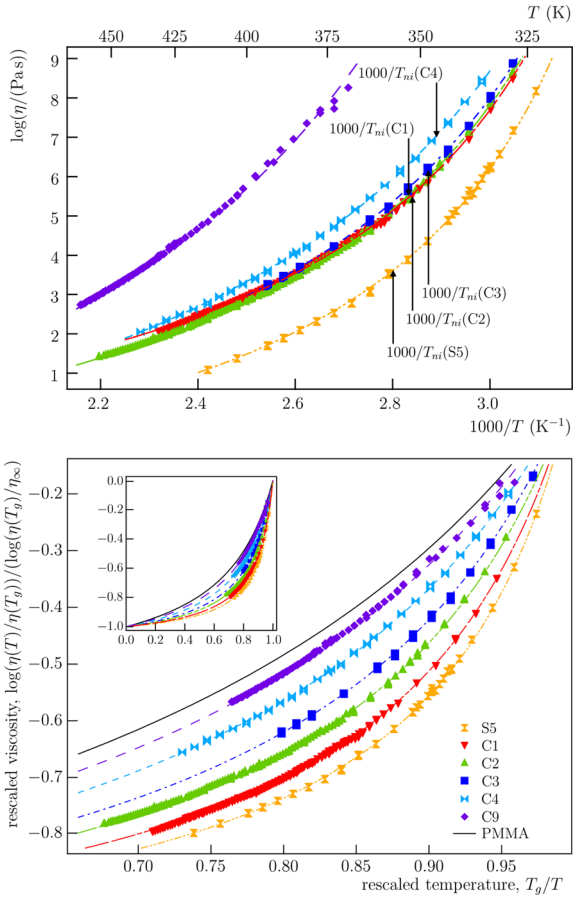

Figure 2. Top: viscosity of PMA4 samples as a function of $1000/T$; the T_{ni} temperatures are also marked. Bottom: logarithm of the rescaled viscosity $(\eta(T)/\eta(T_g))^{(T_g-T_0)/T_b}$ of PMA4 samples as a function of T_g/T; the rescaled viscosity of a PMMA homopolymer[54] is also shown.

dx.doi.org/10.1021/ma400260n | Macromolecules 2013, 46, 5003−5017

Table 2. Zero Shear Viscosity, VF, and WLF Parameters of PMA4 Samples

sample	T_b (K)	T_0 (K)	T_g (K)	C_1	C_2 (K)	T_r (K)	η_∞ (Pa s)
S1	1300 ± 30	259 ± 5	294	5.5 ± 0.1	101 ± 1	363.0 ± 0.1	(2.2 ± 0.1) × 10^{-3}
S5	1100 ± 30	278 ± 3	305	8.0 ± 0.1	60 ± 1	338.0 ± 0.1	(3.7 ± 0.1) × 10^{-3}
C1	1240 ± 40	274 ± 3	306	6.0 ± 0.1	89 ± 1	363.0 ± 0.1	(5.1 ± 0.6) × 10^{-3}
C2	1480 ± 60	268 ± 3	308	7.5 ± 0.1	85 ± 1	353.0 ± 0.1	(8.8 ± 0.8) × 10^{-3}
C3	1570 ± 30	266 ± 2	314	5.7 ± 0.1	122 ± 2	388.0 ± 0.1	(7.5 ± 0.3) × 10^{-3}
C4	1960 ± 50	258 ± 2	320	5.9 ± 0.1	149 ± 2	407.0 ± 0.1	(2.0 ± 0.2) × 10^{-3}
C9	2680 ± 80	272 ± 3	356	9.0 ± 0.1	133 ± 2	405.0 ± 0.1	(4.1 ± 0.3) × 10^{-4}
PMMA[a]	3530 ± 50	286 ± 1	390	8.7 ± 0.1	176 ± 1	463.2 ± 0.1	–

[a]Data from ref 54.

For every sample, the viscosity was fitted by means of a single Vogel–Fulcher law (VF)[52]

$$\eta(T) = \eta_\infty \exp\left(\frac{T_b}{T - T_0}\right) \tag{16}$$

The best fits are superimposed to the experimental curves in Figure 2. Pseudoactivation energies T_b and Vogel temperatures T_0 are given in Table 2. The values of η_∞, partially published elsewhere,[53] are also reported for completeness purposes.

In some literature studies on side-chain liquid-crystalline polymers, a discontinuity at T_{ni} in the slope of $\eta(T)$ was observed,[48,49] and the viscosity was found to follow different Arrhenius laws in the nematic and the isotropic phases, with the activation energy in the nematic phase being higher than in the isotropic one. For PMA4 polymers of the present work, the Stickel plot[55] representation of the viscosity,[56] $[d[\log \eta]/d(1/T)]^{-1/2}$ versus $1000/T$, confirms a single VF behavior, as is shown in Figure 3, for the selected cases of homopolymer S5 and copolymer C4.

Because a VF trend guarantees, as a mathematical consequence, the slope of $\eta(T)$ in the nematic phase to be higher than in the isotropic one, the two contiguous activated regimes of ref 49 could be reconciled with the VF behavior of the PMA4s viscosity by considering the greater fragility of PMA4 homopolymers[53] and the wider ranges of temperature measured for PMA4s with respect to the 30 K range at most of those literature studies: indeed small temperatures ranges could show the intrinsic VF curvature as two activated regimes. This interpretation is supported also noting that a single temperature dependence for the diffusion coefficient was found in ref 48: this turns out to be at variance with the two contiguous activated regimes of η, because η and the diffusion coefficient have the same temperature dependence as the monomeric friction factor.[36,57]

In dynamic experiments, no heterogeneous behavior was observed either. Moreover, all the samples showed superimposable dynamic moduli G' and G'' as a function of the frequency at temperatures below and above the nematic-to-isotropic transition, and also across the conformational transition for the homopolymers.[58] Accordingly, the validity of TTS allowed us to build the master curve (in Figure 4 examples for S1 and C9 samples) and to collect the horizontal shift factors $a_{T_r}(T)$ for each sample. The $a_{T_r}(T)$ were fitted with the Williams–Landel–Ferry (WLF) law:[59]

$$\log a_{T_r}(T) = -\frac{C_1(T - T_r)}{C_2 + T - T_r} \tag{17}$$

whose parameters are given in Table 2.

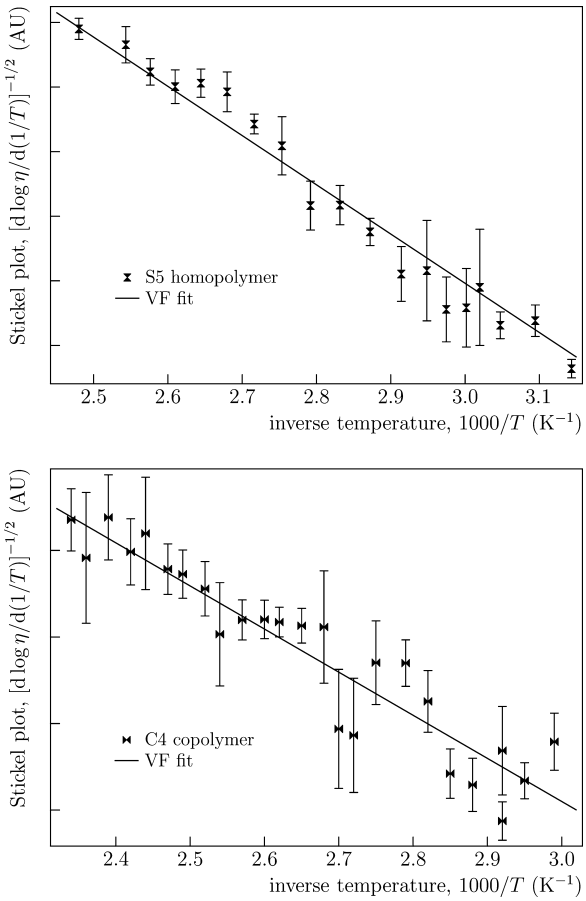

Figure 3. Stickel plot of zero-shear viscosity of S5 and C4.

The validity of TTS with $b_{T_r} \cong 1$ in materials has as a general consequence that VF parameters of the viscosity can be related to T_r-independent parameters of WLF by means of[36,53,57]

$$C_1 C_2 \ln 10 = T_b \tag{18a}$$

$$T_r - C_2 = T_0 \tag{18b}$$

Inspection of Table 2 confirms that these relationships are fulfilled, and further supports the TTS effectiveness in PMA4 polymers in the investigated ranges of frequency and temperature.

Actually, the validity of the TTS could be quite unexpected for the liquid-crystal polymers PMA4 of this work. In fact, when the polymer architecture induces heterogeneous backbone dynamics, TTS failures are widely predictable, because main-chain normal modes are characterized by different monomeric friction coefficients, which may have a different temperature-

dx.doi.org/10.1021/ma400260n | Macromolecules 2013, 46, 5003–5017

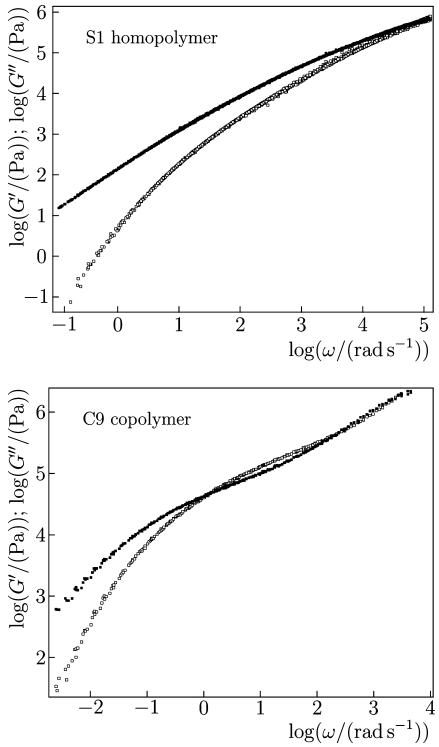

Figure 4. Master curves of S1 and C9 samples (open symbols: storage modulus).

dependence. This inhibits the possibility of a unique temperature scaling of different normal modes, and the heterogeneous nature of such a polymer should become apparent for rheological modes with typical lengths[10] comparable or smaller than the length of the dynamic units.

As a matter of fact, failure of TTS is found in literature studies of diblock copolymers,[60] because of the presence of heterogeneous dynamic units. Nevertheless, TTS held[61] for those rheological modes extending over such a length scale that the mode dynamic units turned out to be homogeneous. Moreover, numerical studies showed that well-defined domains with narrow interfaces are missing in random copolymers,[62] differently from the classic microphase of diblock copolymers, where distinct values of counit densities are present in regions locally rich in one of the two counits.

These considerations can justify the occurrence of TTS in PMA4 polymers, since an average monomeric friction coefficient, determining the temperature dependence of material functions and main-chain dynamics, might be assumed over lengths typical of modes effective from a few degrees above T_g.

Besides the copolymer nature, the liquid-crystalline character of the PMA4 random copolymers could also affect the validity of TTS. It is known, for example, that the configuration of main-chain liquid-crystal polymers is greatly modified in the nematic phase, and the pertinent oscillatory material functions generally depend on shear stress/strain and thermal history of the sample. Failures of TTS have been found in main-chain liquid-crystal polymers,[63] while studies on nematic side-chain polymers have shown breakdown of the TTS at very high masses, in presence either of entanglement[64,65] or nematic groups localized "far" enough from the polymer backbone,[66] also depending on the main-chain architecture.[67]

On the other hand, TTS held in polyacrylates and polymethacrylates similar to the present PMA4s, with mesogenic azobenzene side groups and comparable weight-average molar-masses.[48] Despite their high molar mass, those polymers appeared to be unentangled. These literaure results agree with the TTS effectiveness on PMA4 polymers of this work, which show unentangled master curves, and substantiate the validity of TTS from a different perspective.

4.2. Calculation of the Complex Shear Modulus According to Literature Dynamic Models. Inspecting the master curves (Figures 5−8), it is seen that PMA4 polymers of this work apparently show unentangled master curves, except for C9, the copolymer with less abundance of MA4 counit. Key features of entanglement in G^* curves could have been expected on the sole basis of the high molar masses of PMA4s; for every polymer of the series, these could be estimated greater than the M_e values, after comparing each M value of PMA4 with the value of the entanglement mass of PMMA homopolymer. The lack of entanglement plateau in these side-chain nematic polymers is usually ascribed to the mesophase order that would dilate the confining tube, on whose dimension the M_e value depends,[48,68] and would shift entanglement to higher molar masses. High values of M_e were also found in other side-chain liquid-crystalline polymethacrylates.[64]

Interesting in-depth tests of the dynamic models presented in the previous theoretical section can be carried out starting from the master curves of PMA4 polymers. In fact, ordinary models of polymer dynamics could be inadequate for such polymers, in spite of the TTS validity. Drawbacks could also originate from the lack of the entanglement plateau in the master curves of G^*, despite the high molar masses of most of the PMA4s. Moreover, their high polydispersity could cause the mixing rules to fail in these melts.[69]

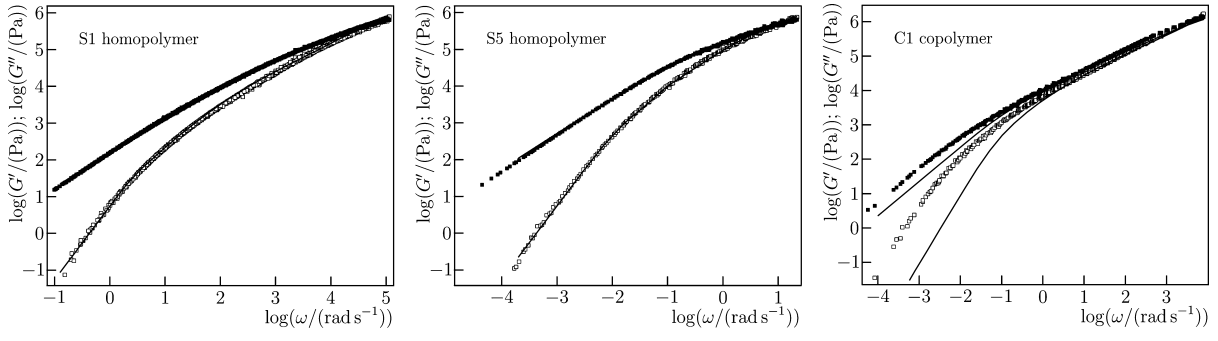

Figure 5. Master curves of S1, S5, and C1 according to the Rouse model for unentangled chains (UR) in comparison with the experimental results.

dx.doi.org/10.1021/ma400260n | Macromolecules 2013, 46, 5003−5017

Table 3. Fitting Parameters for PMA4 Samples with a Single Monomeric Friction Coefficient and χ_r^2 Value of the Best Fit. The Value of the Rouse Time at M_w is Also Provided

sample	x	K_R (μs)	M_e (kg mol^{-1})	ν	χ_r^2	τ_R (M_w) (s)
S1	0.0	1.5×10^{-1}	>200[a]	–	0.2	1.0×10^{-2}
S5	0.0	7.7×10^{1}	>400[a]	–	0.3	7.5
C1	0.1	1.8×10^{0}	450	0.100	1.5	1.3
C2	0.2	1.1×10^{1}	375	0.208	1.0	9.1
C3	0.3	1.6×10^{-1}	255	0.165	0.9	6.8×10^{-2}
C4	0.4	2.8×10^{-2}	165	0.166	0.8	1.0×10^{-2}
C9	0.9	2.3×10^{0}	23.2	0.127	0.5	1.4
PMMA[b]	1.0	3.0×10^{-1}	10.5	0.224	0.3	–

[a]Fits according to both UR and DECLF models provide the same K_R values for S1 and S5. Moreover, because of the unentangled behavior of the homopolymers, we are only able to provide the DECLF model bounds for M_e, which is expected to be higher than the highest component of the molar-mass distribution of S1 and S5. [b]Data from ref 54.

The first attempt of calculating master curve was performed excluding any reptation model from the fitting algorithm, as naively inferred by the lack of entanglement plateau. Therefore, the simulation of master curves was carried out only by means of the Rouse model for unentangled chain (UR). In Figure 5, superposition of experimental and calculated master curves for S1, S5, and C1 samples is shown. Good agreement of experimental and theoretical curves is found for the homopolymers.[70] This finding evidenced that the entanglement mass M_e of S1 and S5 is higher than the highest appreciable M content of the molar mass distributions. Consequently, it was possible to determine the bulk density ρ and the K_R coefficient (see eqs 1 and 2) with minimization of χ_r^2, where $G^*_{th}(\omega)$ was obtained analytically, according to the UR model. The values of K_R for S1 and S5 are given in Table 3. Regarding the bulk density of the PMA4 homopolymers, a common value was found: $\rho \cong 1.1$ g cm^{-3}. This value is also similar to the one reported in literature for PMMA homopolymers, 1.13 g cm^{-3}.[68] On these bases, a unique value of $\rho \cong 1.1 \pm 0.1$ g cm^{-3} was assumed for all the polymers PMA4 in all the calculations of the present work.

The good results obtained with the calculations for the homopolymers imply that the linear mixing rule of eq 13 holds for these polydisperse samples. However, from Figure 5 it is apparent that Rouse model fails to provide good-quality fits in the whole PMA4 series. The UR failure in reproducing the C1 copolymer case suggests that reptation mechanisms may be expected even when no obvious evidence of entanglement plateau in the experimental master curves of G^* occurs.

This behavior is general and well-known in the literature,[57,71,72] and it caused the issue of the precise determination of the onset of entanglement to arise.[68,71,73,74] Many researchers dealt with this topic of polymer dynamics, studying the onset of entanglement with various techniques, including magnetic resonance,[75] neutron scattering,[76] and dielectrometry.[77] In particular, rheology investigations looked for changes in the mass dependence of some material functions,[10,36,54,57,71,78,79] namely the shear modulus. It was shown[71,72] that calculation of G^* definitely provides a signature for a crossover from unentangled to entangled behavior at M_e, as determined by the models described above in the theoretical section. Consequently, our algorithm was implemented with reptation models via eq 13. The substantial equivalence of the DE, DECLF, and TDD models without constraint release, and of ER3 and ER5 models was verified for all the PMA4 samples of this study, and is shown in Figure 6 for the case of copolymer C1.

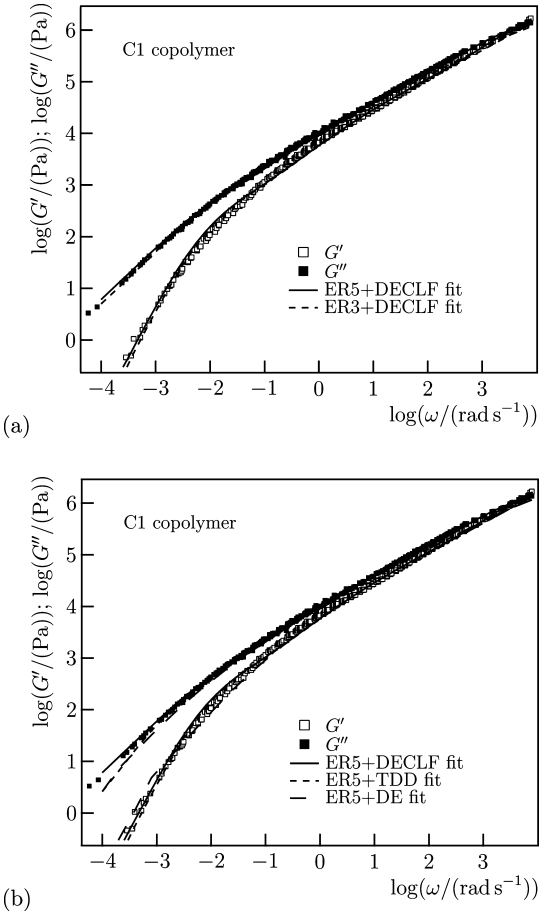

Figure 6. Comparison of experimental and calculated master curves of C1. In part a, the experimental data are compared with calculations obtained via eq 13 according to the DECLF reptation model without CR and Rouse relaxation employing ER3 or ER5. In part b, theoretical curves are obtained mixing the Rouse relaxation, ER5, with reptation models (DE, DECLF, TDD) without CR.

The practicability of neglecting constraint release and of adopting a single-reptation[21] approach is consequent on the mesogenic order of the side chains, which dilates the reptation tube. In a "fully dilated" regime,[16] chains reptate in a "supertube"[16] of permanent obstacles, and the fastest mode of chain relaxation is the chain reptation through fixed obstacles, which just correspond to the assumptions of the reptation model by Doi and Edwards.[10,16] The presence of tube dilatation is inferred from the unentangled aspect of the PMA4s

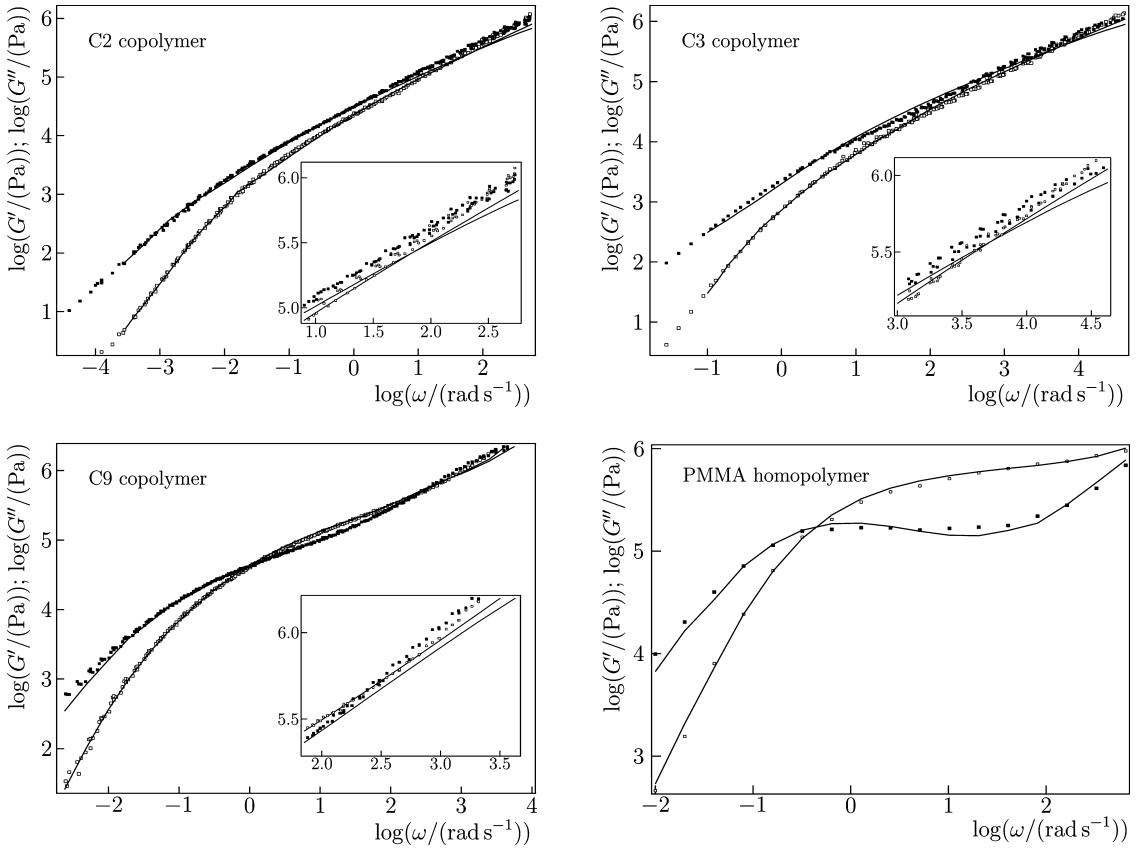

Figure 7. Master curves of C2, C3, and C9 copolymers. Experimental results are superimposed to fit curves (continuous line) obtained via eq 13 with a single average monomeric friction coefficient (aDECLF in section 4.2). PMMA master curve from the literature[54] is also given. Insets show the high-frequency side of the master curves for copolymers. Master curves and simulation of S1, S5 are given in Figure 5, of C1 in Figure 6, and of C4 in Figure 8.

master curves (Figures 5−8): the more the MA4 content, the more the unentangled behavior is apparent despite the high molar mass.

Therefore, the master curves of PMA4 polymers were calculated via eq 13 using the combination of ER5, and DECLF models, without the inclusion of CR. The disengagement time τ_d was set by eq 5, without introducing any empirical $\tau_d \propto M^{3.4}$ dependence on the mass, often employed for better quality fits.[19] In this way, the number of free parameters in the fitting procedure was limited to 3, namely K_R of eq 2, the entanglement mass M_e, and the ν parameter of eq 7. We will refer to this combination as "aDECLF".

In Figure 7, the theoretical curves for G^* are superimposed to the experimental master curves, while in Table 3, fitting parameters are given together with the chi squared values χ_r^2, that were found to be lower than 1.5. By inspection, the good agreement of calculated and experimental data can be appreciated, and confirms the absence of constraint release mechanisms because of the liquid-crystalline order of the melts.

From data in Table 3, it turned out that the value of the entanglement mass M_e was higher than 400 kg mol^{-1} for the homopolymers, with values decreasing with the decreasing liquid-crystalline order from homopolymers S1 and S5 to 23.2 kg mol^{-1} for copolymer C9. Note that possible shifts in the absolute value of M in eq 13 result in the same amount of shift for the absolute M_e value, but turn out ineffective in relative estimations, such as M_e/M_w. A comparison with M_e literature values for entanglement mass of homopolymer PMMA (about 10 kg mol^{-1})[68] confirms the effects of the liquid-crystalline order on the tube topology and entanglement dynamics.

As a final remark, data reported in Tables 1 and 3 allow the calculation of a M_e/M_w ratio of 3 for the copolymers (except C9), and even higher for the two homopolymers. On this basis, one could argue that UR model itself should be enough to provide good theoretical curves of the experiments. Actually, agreement between UR predictions and experimental master curves was only satisfactory for the homopolymers (Figure 5). Even if $M_e > 3M_w$ for copolymers C1−C4, reptation dynamics was needed to obtain good fits for their master curves because of the sample polydispersity, which provides a significant molar-mass content exceeding M_e.

4.3. Calculation of Complex Shear Modulus Taking Randomness into Account. The reduced χ_r^2 of calculated master curves of PMA4 polymers was lower than 1.5. However, a better agreement was obtained between the theoretical and experimental data in copolymers on the low frequency region. For instance, the best fit simulation of sample C4 showed a χ_r^2 lower than 0.5 in the low frequency region, and about 2.0 in the high frequency range (Figure 8). This suggests that drawbacks are present at the fastest correlation times, corresponding to the shortest dynamic modes (namely, high p in dynamic core functions), where the Rouse theory is effective.

The result can be understood considering that the chains do not belong to homopolymers, but are constituted of counits, whose monomeric friction coefficient is expected to depend on the chemical composition and architecture of each bead originating the mode. Because of randomness of the copolymer,

dx.doi.org/10.1021/ma400260n | Macromolecules 2013, 46, 5003−5017

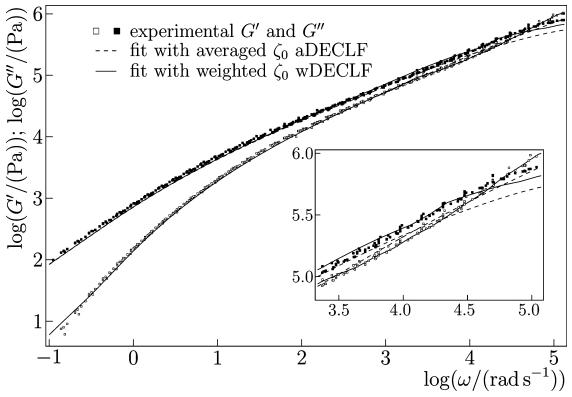

Figure 8. Comparison of experimental data and calculations with aDECLF (dashed line) and wDECLF (continuous line) monomeric models for copolymer C4.

a single average value of the monomeric friction coefficients is not sufficient to express the real composition of the units contributing to the modes. In fact, simple statistical considerations demonstrate that a fluctuation from the average composition in copolymers can change heavily the monomeric friction coefficient. Numerical studies[62] showed how the density of a certain counit in random copolymer melts is characterized by a broad distribution of probability, which depends on the examined cell size.

The probability to have k MMA counits among the n total counits of a portion of chain is

$$P(n, k) = \binom{n}{k}(1 - x)^{n-k}x^{k} \tag{19}$$

where x is the probability to find an MMA counit in the melt (e.g., 0.4 in C4). Therefore, nx units of MMA are expected on the average, among n counits. For high index dynamic modes, namely when the dynamic units are small portions of chain, it is possible to find, at fixed n, a probability near to the one of the mean value (namely nx) also for k values significantly different from nx itself.

To clarify the problem, the case of C1 (x = 0.1) is shown in the following sketch, for the dynamic mode involving 10 counits of the main chain:

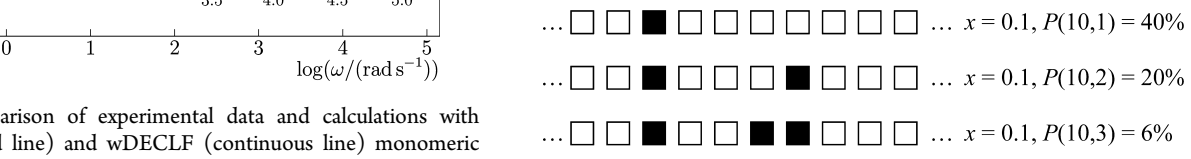

The probability to have a mode of 10 counits with 1 MMA counit (the average case) is 40%, while the probability to find 2 MMA counits in the same mode is 20%, which is not negligible with respect to the previous case.

In order to take into accounts for randomness, the monomeric friction coefficient in eqs 5, 7a and 7b was modified as a weighted monomeric friction coefficient:

$$\zeta_0 = \frac{n - k}{n}\zeta_0^{\mathrm{MA4}} + \frac{k}{n}\zeta_0^{\mathrm{MMA}} \tag{20}$$

with ζ_0^{MMA} and ζ_0^{MA4} monomeric friction coefficients of MMA and MA4 counits, respectively. Moreover, the realization probability of the different modes was considered, by substituting the dynamic cores of the dynamic models, such as, for example, the simple exponential decay in eq 1, with

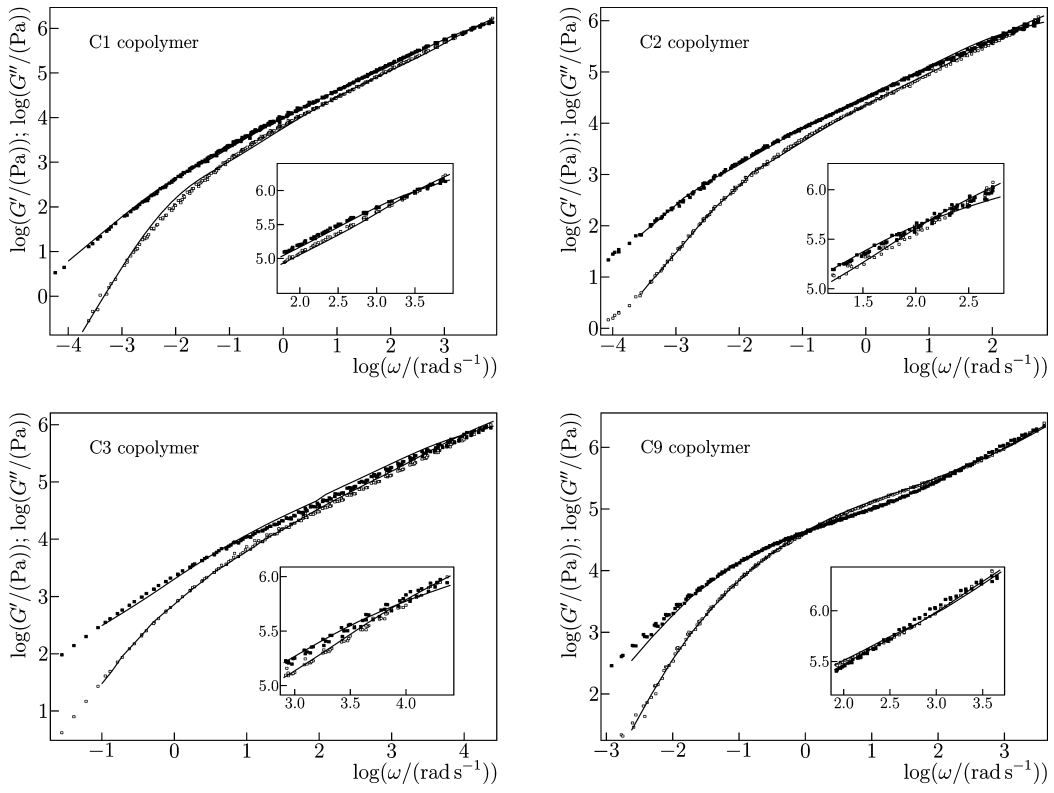

Figure 9. Master curve calculations of PMA4 copolymers. The case of C4 is reported in Figure 8. The fits were obtained according to the wDECLF model with the weighted monomeric friction coefficient of eq 20.

dx.doi.org/10.1021/ma400260n | Macromolecules 2013, 46, 5003−5017

Table 4. Fit Parameters for Polymers PMA4 Calculated According to the wDECLF Model and Monomeric Friction Coefficients[80] of MMA and MA4 at $T = T_g + 100$ K

sample	x	K_R^{MMA} (μs)	K_R^{MA4} (μs)	χ_r^2	ζ_0^{MMA} (kg s^{-1})	ζ_0^{MA4} (kg s^{-1})
S1	0.0	–	1.5×10^{-1}	0.2	–	4×10^{-9}
S5	0.0	–	7.7×10^{1}	0.3	–	3×10^{-9}
C1	0.1	5.4×10^{0}	1.4×10^{0}	0.4	4×10^{-8}	8×10^{-9}
C2	0.2	3.4×10^{1}	5.4×10^{0}	0.3	3×10^{-8}	3×10^{-9}
C3	0.3	3.6×10^{-1}	7.0×10^{-2}	0.5	3×10^{-8}	4×10^{-9}
C4	0.4	5.1×10^{-2}	1.3×10^{-2}	0.3	1×10^{-8}	3×10^{-9}
C9	0.9	2.6×10^{0}	7.6×10^{-1}	0.4	3×10^{-8}	7×10^{-9}
PMMA[a]	1.0	3.0×10^{-1}	–	0.3	2×10^{-8}	–

[a]Data from ref 54.

$$\ldots \sum_{p} \sum_{k=0}^{n} P(n, k) \exp\left(-\frac{p^2 t}{\tau}\right) \tag{21}$$

where $n = M/(pM_0)$ is the number of segments involved in the pth mode (M_0 is the average molar mass of dynamic units).

Using the weighted monomeric friction coefficient correction and the composition distribution of the modes eq 21 and eq 19, an appreciable improvement of the fits was obtained in the high frequency region, as is seen for the whole copolymer series in Figure 9 and in Figure 8, in the latter in comparison with the aDECLF model. χ_r^2 was found to be lower than 0.5 in the whole frequency range (Table 4). We will refer to this model with weighted monomeric friction coefficient as "wDECLF".

The new simulations did not change the outcomes of M_e values, as well as the ν parameters, because in the entangled modes the fluctuations from the average composition of the copolymers are by far less probable. Therefore, a single average monomeric friction coefficient is able to reproduce the shear complex modulus G^* in the low frequency region. Similarly, the terminal zone obtained in the new simulations, which has identical value to the previous one, implies that the weighted monomeric friction coefficient turns out to be equal in this low frequency region to the average monomeric friction coefficient used in previous calculations of G^*.

The K_R coefficients of MMA and MA4 counits, just like obtained as free parameters from the fitting procedures, are given in the third and fourth columns of Table 4. From them, the values of monomeric friction coefficients of MMA and MA4 can be retrieved (see eq 2) and profitably compared, after a shift to the same temperature $T = T_g + 100$ K employing TTS (Table 4). The monomeric friction coefficient ζ_0^{MA4} was found to be the same throughout the series, $(5 \pm 2) \times 10^{-9}$ kg s^{-1}. Likewise, ζ_0^{MMA} has the same value throughout the series, very similar to literature data found for PMMA homopolymers, $(2.0 \pm 0.6) \times 10^{-8}$ kg s^{-1}.[36,54] As a final remark, the relative error over the evaluation of ζ_0^{MA4} and ζ_0^{MMA}, 40% and 30%, respectively, includes the effects of possible shifts in the absolute value of M.

4.4. Entanglement, Packing-Length and MML Model. The M_e data calculated for PMA4 samples can be used to test an empirical model, widely employed in the literature, namely the packing model.[68,74] The packing concept combines entangling properties of the chain with its coiling properties. Studies on different polymer melts have shown[68,74] the existence of universal empirical laws linking entanglement parameters, such as M_e, and microscopic quantities. All the macromolecular information is contained in the definition of packing length $\hat{p}$:

$$\hat{p} = \frac{M_0}{b^2 N_A \rho} \tag{22}$$

This expression relates $\hat{p}$ to the effective bond length b and to the average molar mass M_0 per backbone bond via the polymer density ρ and the Avogadro number N_A. Within the framework of the packing model, the following empirical expression has been developed relating the packing length to the entanglement molar mass:[68,74]

$$M_e = 361.9 N_A \rho \hat{p}^3 \tag{23}$$

Equation 23 provides high values of the packing lengths (Table 5) of the polymers PMA4 with respect to ordinary flexible polymers,[68] because of the high M_e values obtained for polymers PMA4 with the aDECLF model (Table 3).

Table 5. Packing Lengths of PMA4 Samples and PMMA

sample	x	M_e (kg mol^{-1})	$\hat{p}^3$ (Å^3)	$\hat{p}$ (Å)	$\hat{p}^{PMMA}$ (Å)	$\hat{p}^{PMA4}$ (Å)
S1	0.0	>200	>800	>9.3	–	>9.3
S5	0.0	>400	>1600	>11.7	–	>11.7
C1	0.1	450	1800	12.2	3.43	13.1
C2	0.2	375	1500	11.4	3.43	13.4
C3	0.3	255	1000	10.1	3.43	12.9
C4	0.4	165	660	8.7	3.43	13.0
C9	0.9	23.2	93	4.5	3.43	13.4
PMMA[a]	1.0	10.5	42	3.5	3.43	–

[a]Data from ref 54.

On the other hand, starting from the values of $\hat{p}^{PMMA} = 3.43$ Å for PMMA, as evaluated in refs 68 and 74, and the packing length $\hat{p}$ of the PMA4 copolymer series (Table 5), the value of $\hat{p}^{PMA4}$, packing length of the homopolymers PMA4, can be derived from:

$$\hat{p} = x\hat{p}^{PMMA} + (1 - x)\hat{p}^{PMA4} \tag{24}$$

which expresses the packing length of the copolymer PMA4 series as a function of x, the mole fraction of MMA counits. An average value of about 13.2 Å is found for $\hat{p}^{PMA4}$.[81] Figure 10 shows M_e versus the mole fraction x and its best fit carried out, according to eq 23 and eq 24, with $\hat{p}^{PMA4}$ as free parameter. It gives: $\hat{p}^{PMA4} = 13.1$ Å.[81] From eq 23 and Figure 10 it is seen that M_e values could be confidently estimated for any copolymer composition.

SANS studies on two homologous side-chain liquid crystalline polymethacrylates structurally related to PMA4 polymers of this work reported that $\hat{p}$ increased from about 10−11 Å, on increasing the length of the terminal alkyl tail on

dx.doi.org/10.1021/ma400260n | Macromolecules 2013, 46, 5003−5017

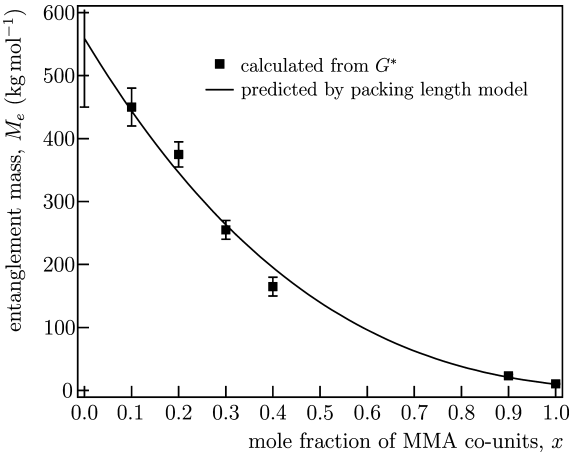

Figure 10. Plot of entanglement mass for PMA4s as a function of x, namely the mole fraction of MMA counits. The superimposed line is the best fit according to eqs 23 and 24.

the mesogenic unit from methyl to butyl.[82] Thus, the value of $\hat{p}$ evaluated for the present homopolymers, carrying a longer pentyl terminal alkyl tail, is in agreement with that trend of dependence of packing length with the molecular structure of the mesogenic repeat unit.

The packing-length approach gives back an estimation of the entanglement mass of PMA4 homopolymers, as shown in Figure 10 and Figure 11. In the latter, M_e is plotted as a

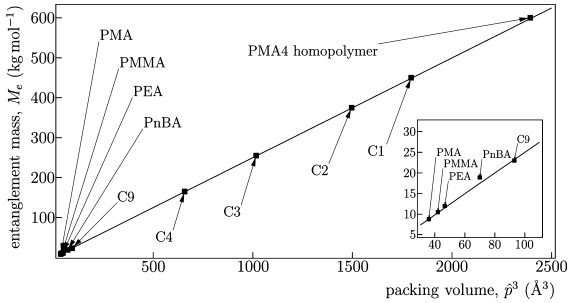

Figure 11. Plot of entanglement mass against the third power of packing volume. Data for PMA4s studied in this work and for literature poly(alkyl acrylate)s[57,83] and PMMA[54] fit the expected $\hat{p}^3$ power law of eq 23. The inset highlights the low M_e region.

function of $\hat{p}^3$ for PMA4 homo- and copolymers together with literature PMMA[54] and more poly(alkyl acrylate)s[57,83] that all well agree with the linear dependence of eq 23.

An evaluation of the effective bond length b for the PMA4 homopolymers can be given via eq 22, providing b = 5 Å.[81] Then, it is possible also to estimate the Flory characteristic ratio[10] C_∞, defined as the square of the ratio b/l_0, where l_0 is the length of the bond in the main chain. It is found that C_∞ = 11.1. Such a value is quite similar to literature side-chain liquid-crystalline polymethacrylates with methyl-terminated side-chains similar to PMA4s of this work,[82] which showed a Flory characteristic ratio about 12.5.

Information on other molar masses related to entanglement and reptation, namely the critical mass M_c and the pure reptation mass M_r, could also be inferred from dynamics models. The pure reptation mass M_r is defined as the molar mass at the crossover between two regimes of the viscosity with the mass, namely the contour-length fluctuation regime where $\eta(M) \sim M^{3.4}$ and pure reptation one, where $\eta(M) \sim M^3$. The critical mass M_c is usually associated with M_e in ordinary entangled polymers by means of the empirical law M_c/M_e = 2.0−2.2, and defines the crossover from the Rouse mass-dependence of the viscosity to the $M^{3.4}$ regime.[36,57,78] Accordingly, it is possible to write[74] for $\eta(M)$ above M_c

$$\eta(M) = \eta(M_c)\left(\frac{M}{M_c}\right)^{3.4} \tag{25}$$

Expressions of $\eta(M)$ different from eq 25 have been provided in the literature,[78] which result in slight changes of the values of M_c. Moreover, other definitions for critical masses were given as the masses at which the entangled behavior becomes apparent in the materials functions of ordinary flexible polymers,[54,57] such as the first appearance of the entanglement plateau in G^* master curves. This led to consider the critical mass M_c as an effective entanglement mass, even if, unlike M_e, no model is able to provide any microscopic definition of M_c.

Actually, a relationship among M_c, polymer molar mass and radius of gyration, was proposed in literature,[84] that can be reformulated in terms of the parameters of the packing-length model as[74]

$$M_c = M_e\left(\frac{9.2\ \text{Å}}{\hat{p}}\right)^{0.65} \tag{26}$$

According to eq 26, the entanglement and the critical molar mass M_c become equal at $\hat{p}$ = 9.2 Å. In the cases of C1−C3 copolymers, eq 26 gives M_c values lower than M_e. In literature three polymer species are also reported with $M_e > M_c$ as drawn from eq 26.[74] The authors suggested that this unusual result would give the opportunity to explore the implications of eq 26 itself.[74] Actually, controversies could arise in applying the empirical law of eq 26 to polymers PMA4, because it was originally derived from fitting experimental data of ordinary flexible polymers.[74,85] Furthermore, in the past decade studies have shown[71] that the Rouse model fails in describing the complex modulus at the entanglement mass, then decreasing the role of the empirical quantity M_c. In addition, it could be questioned about the ability of a microscopic model, such as the packing-length model, to reproduce a fully empiric parameter such as M_c.

Consequently, to get more insight about M_c in PMA4 polymers, we consider a different literature model, the MML model,[20] able to provide the crossover of $\eta(M)$ from Rouse to reptation regimes without introducing any M_c.[20] Following this model, it is possible to calculate $G(t)$ analytically, when constraint release mechanism is not taken into account. In such a way the calculation of $\eta(M)$ only depends on K_R and M/M_e, and no further assumptions are needed about reptation parameters.[86] Accordingly, $\eta(M)$ was determined for PMA4 homopolymers, considered as monodisperse, as the integral $\int_0^\infty G(t)dt$. The resulting curve is shown in Figure 12, where the experimental points corresponding to the masses of the homopolymers of this work are also superimposed. The presence of an M_c at about 2 M_e is apparent. This result is in accordance with the findings in ordinary flexible polymers[57,74] for M_c and is at variance with the predictions of eq 26. It seems therefore that, even if both packing-length model and the MML dynamic model work for PMA4 polymers with reference to M_e, at least one of the two models fails in predicting M_c.

dx.doi.org/10.1021/ma400260n | Macromolecules 2013, 46, 5003−5017

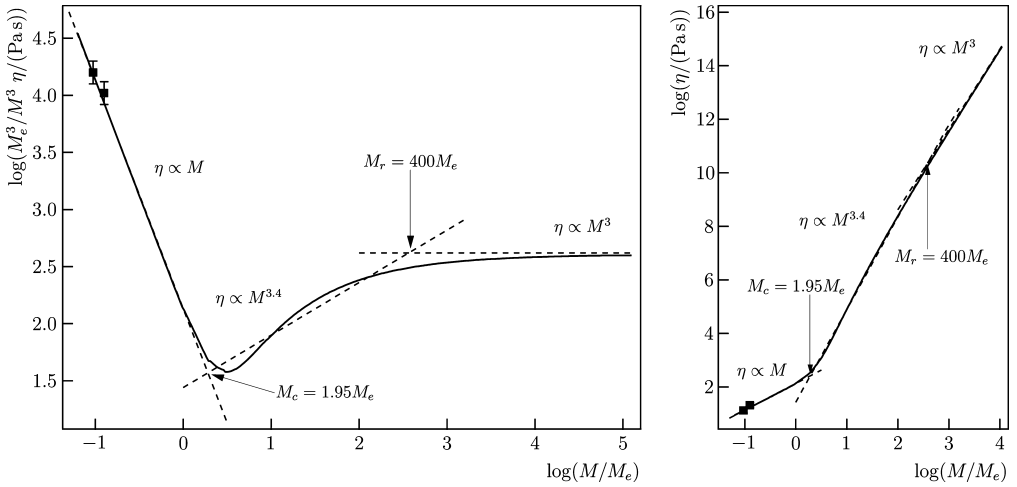

Figure 12. Mass dependence of viscosity for PMA4 homopolymers as evaluated according to the MML model at T_g + 100 K. Experimental data of S1 and S5 at T_g + 100 K are also superimposed in correspondence of their M_w. The rescaled η/M^3 plot (left side) is more effective in highlighting details with respect to the η versus M graph (right side).

As far as the reptation mass M_r is concerned, it signals the crossover from a regime where contour-length fluctuations are active to a pure reptation regime for very long chains, where fluctuations contribution is reduced[10,20] and $\eta(M) \propto M^3$. Such a behavior is seen in Figure 12, where, according to the MML model, η/M^3 becomes a constant for sufficiently high molar masses.

Analytically the reptation mass can be defined as[13,87]

$$\eta(M) = \frac{12}{5}\frac{M^3}{M_c M_e^2}\eta(M_c) \tag{27}$$

When $\eta(M_r)$ from eq 25 equals $\eta(M_r)$ from eq 27, the relationship is found[74]

$$\frac{M_r}{M_e} = 7.17\left(\frac{M_c}{M_e}\right)^6 \tag{28}$$

Using the M_c/M_e value found from Figure 12, from eq 28 $M_r/M_e \approx 400$ results, which nicely suits the value extrapolated by Figure 12.

It should be also stressed that the M_c value predicted by the packing-length model via eq 26 would lead to $M_r/M_e < 1$, which is not confirmed in our analysis and never found in the literature. Discrepancies between the expected M_r/M_e ratios evaluated via M_c by eq 26 and experimental ones were also found by Fetters and co-workers.[74]

As a final remark, the experimental viscosity of S1 and S5 at T_g + 100 K is reported in Figure 12, in correspondence of their M_w. The different chain-end free-volume concentration can be neglected at these high molar masses, therefore no correction of experimental data is needed to fit the theoretical curve of Figure 12. The agreement of the experimental data with theoretical values is quite satisfactorily, also in consideration of the high polydispersity of the S1 and S5 samples with respect to the ideal monodisperse behavior modeled by the theoretical curve.

5. CONCLUSIONS

It appears of paramount importance the understanding of the viscoelastic dynamic behavior and of the microscopic dynamics of relaxation of side-chain liquid-crystalline polymers containing the azobenzene moiety in the side chain, which were shown to be a promising medium for optical nanowriting.

Therefore, we focused on a series of homopolymers of an azobenzene methacrylate, with the azobenzene moiety in the side chain, and their random copolymers with different amounts of methyl methacrylate counits. Our work aimed to enlighten the rheological response of the copolymer series with special attention to both the ability of available dynamic models to describe the shear complex modulus and the integration of this information in a consistent network.

Main results can be summarized as follows.

From dynamic experiments at different temperatures, we were able to reconstruct master curves for the complex modulus, evidencing the thermorheological simplicity of the materials. Grounds for occurrence of TTS were discussed, being the result not trivial because of either the copolymer nature or the liquid-crystalline one (or both of these properties) of the series components. Moreover, no evidence of entanglement plateau was observed in the master curves, in spite of the high molar masses of the PMA4s.

Of particular relevance is the investigation regarding the ability of some literature models to reproduce the complex shear modulus. It appeared that the dynamics of these polymers in their nematic phase is similar to ordinary flexible polymers, and can be nicely fitted taking into account entanglement and molar mass distribution. Microscopic information on the materials, such as entanglement molar masses, was obtained in a consistent way, and the macroscopic effects were evidenced of tube dilatation induced by the nematic order on the entanglement plateau of the master curves.

Discrepancies from the experiments observed in the high frequency side of the complex modulus led us to improve the literature models by properly considering the random nature of the copolymers. We were able to retrieve the values of the monomeric friction coefficient of MA4 and MMA counits, the latter resulting in agreement with literature results.

The experimental master curves were also fitted according to the packing-length model. Interestingly enough, it was evidenced the possibility of predicting the viscoelastic behavior of whatever PMA4 random copolymer, provided that the response of the extreme homopolymers of the series had been previously characterized. We provided estimation of the

dx.doi.org/10.1021/ma400260n | Macromolecules 2013, 46, 5003−5017

packing length for all the polymer series as well as the Flory characteristic ratio C_∞ and the effective bond length of PMA4 homopolymers. Finally, information on the critical mass M_c and the pure reptation mass M_r were also inferred from MML model.

In conclusion, the analysis of the rheological response in the linear response regime in terms of dynamic models represents a powerful investigation tool for the homopolymer and random copolymer series of the present work. This approach provides a good starting point for future investigations on copolymer materials where the block architecture and nature are varied to better discriminate the influence of local dynamics (Rouse modes) and collective one over the overall response of the materials.

■ ASSOCIATED CONTENT

Supporting Information

DSC thermograms, examples of amplitude sweeps, and typical flow curves of PMA4s. This material is available free of charge via the Internet at http://pubs.acs.org/.

■ AUTHOR INFORMATION

Corresponding Author

*E-mail: laura.andreozzi@df.unipi.it (L.A.).

Notes

The authors declare no competing financial interest.

■ REFERENCES

(1) Zhao, Y., Ikeda, T., Eds. *Smart Light-responsive Materials: Azobenzene-containing Polymers and Liquid Crystals*; Wiley: New York, 2009.

(2) Priimagi, A.; Ogawa, K.; Virkki, M.; Mamiya, J.; Kauranen, M.; Shishido, A. *Adv. Mater.* **2012**, *24*, 6410−6415.

(3) Bogdanov, A.; Bobrovsky, A.; Ryabchun, A.; Vorobiev, A. *Phys. Rev. E* **2012**, *85*, 011704(7).

(4) Maggini, L.; Marangoni, T.; Georges, B.; Malicka, J. M.; Yoosaf, K.; Minoia, A.; Lazzaroni, R.; Armaroli, N.; Bonifazi, D. *Nanoscale* **2013**, *5*, 634−645.

(5) Tantussi, F.; Menghetti, S.; Caldi, E.; Fuso, F.; Allegrini, M.; Galli, G. *Appl. Phys. Lett.* **2012**, *100*, 083103. Menghetti, S.; Alderighi, A.; Galli, G.; Tantussi, F.; Morandini, M.; Fuso, F.; Allegrini, M. *J. Mater. Chem.* **2012**, *22*, 14510−14517 and references therein..

(6) Andreozzi, L.; Faetti, M.; Galli, G.; Giordano, M.; Palazzuoli, D. *Macromol. Symp.* **2004**, *218*, 323−332.

(7) Edwards, S. F. *Proc. Phys. Soc.* **1967**, *92*, 9−16.

(8) De Gennes, P. G. *J. Chem. Phys.* **1971**, *55*, 572−579.

(9) Everaers, R.; Sukumaran, S. K.; Grest, G. S.; Svaneborg, C.; Sivasubramanian, A.; Kremer, K. *Science* **2004**, *303*, 823−826. Pokrovskii, V. N. *Physica A* **2006**, *366*, 88−106. Pokrovskii, V. N. *J. Exp. Theor. Phys.* **2008**, *106*, 604−607.

(10) Doi, M.; Edwards, S. F. *The theory of polymer dynamics*; Oxford University Press: Oxford, U.K., 1986.

(11) Tsenoglou, C. *ACS Polym. Prep.* **1987**, *28*, 185−186.

(12) des Cloizeaux, J. *Europhys. Lett.* **1988**, *5*, 437−442.

(13) Graessley, W. W. *Adv. Polym. Sci.* **1982**, *47*, 67−117.

(14) Ianniruberto, G.; Marrucci, G. *J. Non-Newtonian Fluid Mech.* **1996**, *65*, 241−246.

(15) Marrucci, G. *J. Polym. Sci., Polym. Phys. Ed.* **1985**, *23*, 159−177. Rubinstein, M.; Helfand, E.; Pearson, D. S. *Macromolecules* **1987**, *20*, 822−829.

(16) Viovy, J. L.; Rubinstein, M.; Colby, R. H. *Macromolecules* **1991**, *24*, 3587−3596.

(17) Tsenoglou, C. *Macromolecules* **1991**, *24*, 1762−1767.

(18) Maier, D.; Eckstein, A.; Friedrich, C.; Honerkamp, J. *J. Rheol.* **1988**, *42*, 1153−1173.

(19) van Ruymbeke, E.; Keunings, R.; Stéphenne, V.; Hagenaars, A.; Bailly, C. *Macromolecules* **2002**, *35*, 2689−2699.

(20) Likhtman, A. E.; McLeish, T. C. B. *Macromolecules* **2002**, *35*, 6332−6343.

(21) des Cloizeaux, J. *Macromolecules* **1990**, *23*, 4678−4687. des Cloizeaux, J. *Macromolecules* **1992**, *25*, 835−841.

(22) van Ruymbeke, E.; Bailly, C.; Keunings, R.; Vlassopoulos, D. *Macromolecules* **2006**, *39*, 6248−6259. Padding, J. T.; van Ruymbeke, E.; Vlassopoulos, D.; Briels, W. *J. Rheol. Acta* **2010**, *49*, 473−484. Snijkers, F.; van Ruymbeke, E.; Kim, P.; Lee, H.; Nikopoulou, A.; Chang, T.; Hadjichristidis, N.; Pathak, J.; Vlassopoulos, D. *Macromolecules* **2011**, *44*, 8631−8643.

(23) van Ruymbeke, E.; Keunings, R.; Bailly, C. B. *J. Non-Newtonian Fluid Mechanics* **2005**, *128*, 7−22. van Ruymbeke, E.; Vlassopoulos, D.; Mierzwa, M.; Pakula, T.; Charalabidis, D.; Pitsikalis, M.; Hadjichristidis, N. *Macromolecules* **2010**, *43*, 4401−4411. van Ruymbeke, E.; Coppola, S.; Balacca, L.; Righi, S.; Vlassopoulos, D. *J. Rheol.* **2010**, *54*, 507−538.

(24) Ahmadi, M.; Bailly, C.; Keunings, R.; Nekoomanesh, M.; Arabi, H.; van Ruymbeke, E. *Macromolecules* **2011**, *44*, 647−659.

(25) van Ruymbeke, E.; Nielsen, J.; Hassager, O. *J. Rheol.* **2010**, *54*, 1155−1172.

(26) Arendt, B. H.; Krishnamoorti, R.; Kannan, R. M.; Seitz, K.; Kornfield, J. A.; Roovers, J. *Macromolecules* **1997**, *30*, 1138−1145.

(27) Pattamaprom, C.; Larson, R. G.; Van Dyke, T. J. *Rheol. Acta* **2000**, *39*, 517−553.

(28) Milner, S. T.; McLeish, T. C. B. *Phys. Rev. Lett.* **1998**, *81*, 725−728.

(29) Larson, R. G.; Sridhar, T.; Leal, L. G.; McKinley, G. H.; Likhtman, A. E.; McLeish, T. C. B. *J. Rheol.* **2003**, *47*, 809−818.

(30) In this paper, we follow the "G" convention for the definitions of entanglement spacing and time constants in the tube model treated extensively in ref 29.

(31) Andreozzi, L.; Faetti, M.; Giordano, M.; Palazzuoli, D.; Galli, G. *Macromolecules* **2001**, *34*, 7325−7330.

(32) Angeloni, A. S.; Caretti, D.; Laus, M.; Chiellini, E.; Galli, G. *J. Polym. Sci., Part A: Polym. Chem.* **1991**, *29*, 1865−1873.

(33) Evaluated with ChemSketch.

(34) Zhang, H.; He, W.; Pan, C. *Acta Polym. Sin.* **1999**, *1*, 100−106.

(35) Angeloni, A. S.; Caretti, D.; Carlini, C.; Chiellini, E.; Galli, G.; Altomare, A.; Solaro, R.; Laus, M. *Liq. Crystals* **1989**, *4*, 513−529.

(36) Ferry, J. D. *Viscoelastic Properties of Polymers*; Wiley: New York, 1980.

(37) Andreozzi, L.; Faetti, M.; Giordano, M.; Palazzuoli, D.; Laus, M.; Galli, G. *Mol. Cryst. Liq. Cryst.* **2003**, *398*, 97−106.

(38) Andreozzi, L.; Camorani, P.; Faetti, M.; Palazzuoli, D. *Mol. Cryst. Liq. Cryst.* **2002**, *375*, 129−142. Andreozzi, L.; Faetti, M.; Giordano, M.; Palazzuoli, D.; Zulli, F.; Galli, G. *Mol. Cryst. Liq. Cryst.* **2005**, *429*, 21−29. Andreozzi, L.; Faetti, M.; Giordano, M.; Zulli, F.; Galli, G.; Laus, M. *Mol. Cryst. Liq. Cryst.* **2005**, *429*, 301−312.

(39) Richardson, M. J.; Savill, N. G. *Polymer* **1975**, *16*, 753−757.

(40) Andreozzi, L.; Autiero, C.; Faetti, M.; Giordano, M.; Zulli, F.; Galli, G. *Mol. Cryst. Liq. Cryst.* **2006**, *450*, 363−371.

(41) Morrison, F. A. *Understanding Rheology*; Oxford University Press: Oxford, U.K., 2001.

(42) Zulli, F.; Andreozzi, L.; Passaglia, E.; Augier, S.; Giordano, M. *J. Appl. Polym. Sci.* **2013**, *127*, 1423−1432.

(43) Andreozzi, L.; Faetti, M.; Giordano, M.; Zulli, F. *Macromolecules* **2004**, *37*, 8010−8016.

(44) Honerkamp, J.; Weese, J. *Rheol. Acta* **1993**, *32*, 57−64.

(45) Hiemenz, P. C.; Lodge, T. P. *Polymer Chemistry*, 2nd ed.; Taylor & Francis: Boca Raton, FL, 2007, 486−491.

(46) Scwarzl, F. R. *Rheol. Acta* **1971**, *10*, 165−173.

(47) Nelder, J. A.; Mead, R. *Comput. J.* **1965**, *7*, 308−313.

(48) Colby, R. H.; Gillmor, J. R.; Galli, G.; Laus, M.; Ober, C. K.; Hall, E. *Liq. Cryst.* **1993**, *13*, 233−245.

(49) Zentel, R.; Wu, J. *Makromol. Chem.* **1986**, *187*, 1727−1736.

(50) Lee, K. M.; Han, C. D. *Macromolecules* **2002**, *35*, 6263−6273.

(51) Kresse, H.; Stettin, H.; Tennstedt, E.; Kostromin, S. *Mol. Cryst. Liq. Cryst.* **1990**, *191*, 135−152.
(52) Vogel, H. *Z. Phys.* **1921**, *22*, 645−646. Fulcher, G. S. *J. Am. Ceram. Soc.* **1925**, *8*, 339−345. Tamman, G.; Hesse, W. *Z. Anorg. Allg. Chem.* **1926**, *156*, 245−257.
(53) Andreozzi, L.; Autiero, C.; Faetti, M.; Galli, G.; Giordano, M.; Zulli, F. *Macromol. Symp.* **2008**, *263*, 78−85.
(54) Fuchs, K.; Friedrich, C.; Weese, J. *Macromolecules* **1996**, *29*, 5893−5910.
(55) Stickel, F.; Fischer, E. W.; Richert, R. *J. Chem. Phys.* **1995**, *102*, 6251−6257.
(56) Ngai, K. L. *Relaxation and Diffusion in Complex Systems*; Springer: New York, 2011.
(57) Andreozzi, L.; Castelvetro, V.; Faetti, M.; Giordano, M.; Zulli, F. *Macromolecules* **2006**, *39*, 1880−1889.
(58) Andreozzi, L.; Faetti, M.; Giordano, M.; Zulli, F.; Galli, G. *Mol. Cryst. Liq. Cryst.* **2005**, *441*, 13−26.
(59) Williams, M. L.; Landel, R. F.; Ferry, J. D. *J. Am. Chem. Soc.* **1955**, *77*, 3701−3707.
(60) Hirose, Y.; Urakawa, O.; Adachi, K. *J. Polym. Sci., B: Polym. Phys.* **2004**, *42*, 4084−4094. Park, H. E.; Dealy, J. M. *Macromolecules* **2010**, *43*, 6789−6799.
(61) Kim, E.; Kramer, E. J.; Garrett, P. D.; Mendelson, R. A.; Wu, W. C. *J. Mater. Sci.* **1995**, *30*, 1709−1714. Righetti, M. C.; Munari, A.; Pezzin, G.; Ottani, S. *J. Appl. Polym. Sci.* **1998**, *63*, 1213−1221.
(62) Swift, B. W.; Olivera de La Cruz, M. *Europhys. Lett.* **1996**, *35*, 487−492.
(63) Sun, T.; Lin, Y. G.; Winter, H. H.; Porter, R. S. *Polymer* **1989**, *30*, 1257−1261. Driscol, P.; Masuda, T.; Fujiwara, K. *Macromolecules* **1991**, *24*, 1567−1574. Giamberini, M.; Ambrogi, V.; Cerruti, P.; Carfagna, C. *Polymer* **2006**, *47*, 4490−4496.
(64) Rubin, S. F.; Kannan, R. M.; Cornfield, J. A.; Boeffel, C. *Macromolecules* **1995**, *28*, 3521−3530.
(65) Berghausen, J.; Fuchs, J.; Richtering, W. *Macromolecules* **1997**, *30*, 7574−7581. Hotta, A.; Terentjev, E. M. *Eur. Phys. J. E* **2003**, *10*, 291−301. Auad, M. L.; Kempe, M. D.; Kornfield, J. A.; Rendon, S.; Burghardt, W. R.; Yoon, K. *Macromolecules* **2005**, *38*, 6946−6953.
(66) Lee, K. M.; Han, C. D. *Macromolecules* **2003**, *36*, 8796−8810.
(67) Wewerka, A.; Viertler, K.; Vlassopoulos, D.; Stelzer, F. *Rheol. Acta* **2001**, *41*, 416−425.
(68) Fetters, L. J.; Lohse, D. J.; Richter, D.; Witten, T. A.; Zirkel, A. *Macromolecules* **1994**, *27*, 4639−4647.
(69) Léonardi, F.; Majesté, J.-C.; Allal, A.; Marin, G. *J. Rheol.* **2000**, *44*, 675−692.
(70) Andreozzi, L.; Autiero, C.; Faetti, M.; Galli, G.; Giordano, M.; Zulli, F. *Mol. Cryst. Liq. Cryst.* **2009**, *500*, 63−72.
(71) Lin, Y. H.; Juang, J. H. *Macromolecules* **1999**, *32*, 181−185.
(72) Andreozzi, L.; Autiero, C.; Faetti, M.; Giordano, M.; Zulli, F. *Philos. Mag.* **2008**, *88*, 4151−4159. Lahmar, F.; Tzoumanekas, C.; Theodorou, D. N.; Rousseau, B. *Macromolecules* **2009**, *42*, 7485−7494.
(73) Kremer, K.; Grest, G. S.; Carmesin, I. *Phys. Rev. Lett.* **1988**, *61*, 566−569. Richter, D.; Farago, B.; Butera, R.; Fetters, L. J.; Huang, J. S.; Ewen, B. *Macromolecules* **1993**, *26*, 795−804. Kreer, T.; Baschnagel, J.; Mueller, M.; Binder, K. *Macromolecules* **2000**, *34*, 1105−1117. Tzoumanekas, C.; Lahmar, F.; Rousseau, B.; Theodorou, D. N. *Macromolecules* **2009**, *42*, 7474−7484.
(74) Fetters, L. J.; Lohse, D. J.; Milner, S. T.; Graessley, W. W. *Macromolecules* **1999**, *32*, 6847−6851.
(75) Pearson, D. S.; Verstrate, G.; von Meerwall, E.; Schilling, F. C. *Macromolecules* **1987**, *20*, 1133−1141. Andreozzi, L.; Castelvetro, V.; Faetti, M.; Giordano, M.; Zulli, F. *Philos. Mag.* **2004**, *84*, 1555−1565.
(76) Richter, D.; Ewen, B.; Farago, B.; Wagner, T. *Phys. Rev. Lett.* **1989**, *62*, 2140−2143. Richter, D.; Farago, B.; Fetters, L. J.; Huang, J. S.; Ewen, B.; Lartigue, C. *Phys. Rev. Lett.* **1990**, *64*, 1389−1392.
(77) Adachi, K.; Kotaka, T. *Prog. Polym. Sci.* **1993**, *18*, 585−622.
(78) Colby, R. H.; Fettersqq, L. H.; Graessley, W. W. *Macromolecules* **1987**, *20*, 2226−2237.
(79) Mills, N. J. *Eur. Polym. J.* **1969**, *5*, 675−695. Mills, N. J.; Nevin, A. J. *J. Polym. Sci., Part A−2: Polym. Phys.* **1971**, *9*, 267−281.
(80) The monomeric friction coefficients ζ_0^{MMA} and ζ_0^{MA4} were calculated according to the eq 2: (i) dividing K_R by the b^2 of ref 74. (MMA) or estimated in section 4.4 of this work (MA4); (ii) multiplying the value found in (i) by $3\pi^2 k_B T_r$ obtaining the monomeric friction coefficient at the reference temperature T_r; (iii) rescaling this value to T_g + 100 K by means of the VF law (eq 16) with the VF parameters given in Table 2.
(81) As already stated, possible scaling of $w(M)$ in eq 13 affects the evaluation of K_R and M_e. In the adopted packing-length treatment, M_e only is relevant and possible shifts in its value influence b^2 and $\hat{p}$ as a cube root (eq 23). The subsequent relative error, in the present case about 3%, can be neglected.
(82) Fetters, L. J.; Lohse, D. J.; Graessley, W. W. *J. Polym. Sci., B: Polym. Phys.* **1999**, *37*, 1023−1033 Table IV and references therein..
(83) Andreozzi, L.; Autiero, C.; Faetti, M.; Giordano, M.; Zulli, F. *J. Non-Cryst. Solids* **2006**, *352*, 5050−5054. Andreozzi, L.; Autiero, C.; Faetti, M.; Giordano, M.; Zulli, F. *J. Phys.-Condens. Matter* **2006**, *18*, 6481−6492. Andreozzi, L.; Autiero, C.; Faetti, M.; Giordano, M.; Zulli, F. *Philos. Mag.* **2007**, *87*, 799−810.
(84) Fox, T. G.; Allen, V. R. *J. Chem. Phys.* **1964**, *41*, 344−352.
(85) Wang, S.-Q. *Macromolecules* **2007**, *40*, 8684−8694.
(86) In analogy with the aDECLF and wDECLF models, calculations according to the MML model were done without CR constraining the parameter c_v = 0.
(87) Graessley, W. W. *J. Polym. Sci., Polym. Phys. Ed.* **1980**, *18*, 227−232.